NUMERICAL SIMULATION OF 3-D MIXED-MODE CRACK PROPAGATION ON BIMATERIAL INTERFACES

A. F. Herr & H. F. Nied
Mechanical Engineering and Mechanics, Lehigh University, Bethlehem, PA 18015-3085 USA

ABSTRACT

Numerical simulation of the propagation of an arbitrarily shaped, three-dimensional crack can be a tedious, time-consuming process. This is especially true for 3-D cracks propagating on interfaces between two dissimilar materials. In addition to accurately accounting for the peculiar nature of the crack tip stress field associated with interface cracks, systematic "advancement" of the crack front must be based on an efficient numerical crack advance algorithm. Other important considerations for simulating 3-D crack propagation include: the creation of a solid model, the definition of the crack front, calculation of the stress intensity factors along the crack front, and finally, remeshing in the vicinity of the crack front after each incremental crack advance. In this study, a technique is described that combines the use of the ANSYS finite element software and a specialized finite element program, FRAC3D, developed at Lehigh University, to simulate propagation of arbitrarily shaped 3-D cracks. FRAC3D accurately computes mode I, mode II, and mode III stress intensity factors for 3-D interface cracks. Interface cracks exhibit inherently mixed mode behavior, even when subjected to uniform remote loading normal to the interface. However, when subjected to thermal loading, interface cracking is dominated by mode II and mode III components. The method described in this study uses a modified version of the classical fatigue crack growth rate "law" developed by Paris and Erdogan to simulate stable crack growth under cyclic loading conditions, with the crack constrained to the plane of the interface. As a practical example in semiconductor package reliability analysis, the method is used to simulate crack propagation on a silicon/epoxy interface. Specifically, an interfacial corner-crack subjected to thermomechanical loading. Results from two different initial corner crack shapes are presented and compared. Plots for each show the advancement of the crack front and the changes in the stress intensity factors, strain energy release rates, and phase angles as the crack shape evolves during propagation.

1 INTRODUCTION

In multi-layered composite structures, mechanical integrity is often limited by the adhesive strength of the interfaces between the constituent materials. For example, in electronic packaging, plastic flip-chip packages are fabricated with numerous interfaces between metals, ceramics, and polymers (die/passivation, passivation/underfill, underfill/solder mask, and solder mask/circuit board). These interfaces are often the sites of crack initiation during testing, storage, and device operation. Interfacial delamination between the epoxy underfill material and the silicon die is one of the most commonly observed failure modes and it's generally recognized that accurate modeling of interfacial fracture behavior is crucial for reliable device structural designs [1-2].

Delamination in composite materials usually initiates at corners (Fig. 1). Not surprisingly, this interface debonding corresponds to the singular stress state known to exist at idealized elastic bimaterial corners, and depends on the material properties and the local shape of the corner [2-3]. In this paper, crack propagation is modeled for interface cracks initiating at a corner and propagating on the bond plane between two rectangular slabs of silicon and epoxy. This sort of interfacial cracking is observed in actual electronic packages, as shown in Fig. 1. The sequence of C-SAM acoustic images shown in Fig. 1, depict the progressive interfacial delamination between a silicon die and epoxy underfill, subjected to thermal cycling.

Very few attempts have been made to accurately compute stress intensity factors for 3-D interface cracks at bimaterial corners [2,4-6]. Part of the reason for this is that for interface cracks,

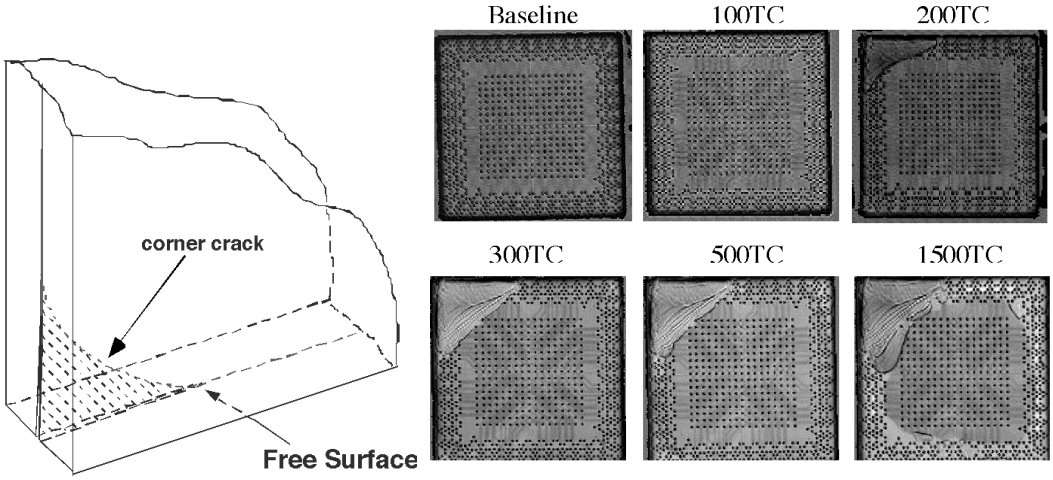

Figure 1: Schematic depicting interface crack advancing on bond plane between two dissimilar materials and a series of C-SAM images showing progressive interfacial delamination, beginning in upper left corner, between a silicon die and epoxy underfill in a microelectronic package. TC indicates the number of thermal cycles. (Courtesy of David Peterson, Sandia National Laboratories).

mode I and mode II stress intensity factors are coupled and do not have the same physical meaning (or units) they have in the homogeneous case [2]. Interface cracks exhibit an oscillatory stress singularity of the form,

$$\sigma_{ij} = \frac{1}{\sqrt{2\pi r}}\left\{ \mathrm{Re}\left[\mathrm{K} r^{i\varepsilon}\right]\tilde{\sigma}_{ij}^{I}(\theta,\varepsilon) + \mathrm{Im}\left[\mathrm{K} r^{i\varepsilon}\right]\tilde{\sigma}_{ij}^{II}(\theta,\varepsilon) + K_{III}\tilde{\sigma}_{ij}^{III}(\theta)\right\} , \tag{1}$$

where r and θ are the local polar coordinates for a coordinate system located on the crack front in planes perpendicular to the crack front. The oscillatory behavior in (1) for small r, arises from the terms, $r^{i\varepsilon} = \cos(\varepsilon \ln r) + i \sin(\varepsilon \ln r)$. In (1), the complex stress intensity factor, $\mathrm{K}=K_I + iK_{II}$, has real and imaginary parts that are somewhat analogous to the conventional mode I and mode II stress intensity factors in homogeneous materials. The functions, $\tilde{\sigma}_{ij}^{I}(\theta,\varepsilon)$, $\tilde{\sigma}_{ij}^{II}(\theta,\varepsilon)$, and $\tilde{\sigma}_{ij}^{III}(\theta,\varepsilon)$, describe the angular distribution of the stress components around the crack tip and are given in [7]. The imaginary power in (1), $r^{i\varepsilon}$, depends on the oscillatory index ε given by

$$\varepsilon = \frac{1}{2\pi}\ln\left[\frac{1-\beta}{1+\beta}\right] , \tag{2}$$

where β is one of two Dundurs' parameters. Dundurs' parameters α and β, quantify the elastic mismatch for bimaterial problems and are given by [8],

$$\alpha = \frac{\mu_1(\kappa_2+1) - \mu_2(\kappa_1+1)}{\mu_2(\kappa_1+1) + \mu_1(\kappa_2+1)} \text{ and } \beta = \frac{\mu_1(\kappa_2-1) - \mu_2(\kappa_1-1)}{\mu_2(\kappa_1+1) + \mu_1(\kappa_2+1)} . \tag{3}$$

In (3), subscripts 1 and 2 refer to the two different elastic materials, $\kappa = 3-4\nu$ (ν is Poisson's ratio), and μ is the elastic shear modulus.

For certain material combinations, β is very small and the coupling between mode I and mode II stress intensity factors can be neglected, as was done in [4]. However, in the case of a silicon/epoxy

interface, the "isotropic" elastic properties of silicon are E_1=128.3 GPa, ν_1=0.28, while the elastic properties of an epoxy underfill material can be given by E_2=12 GPa, ν_2=0.33 [9]. A silicon/epoxy interface with these elastic constants, will have Dundurs' parameters (3) given by α= 0.8235, β =0.2044 and a relatively large oscillatory index (2) ε=-0.066. For such values of β and ε the coupling between the mode I and mode II stress intensity factors should not be ignored.

2 FINITE ELEMENT ANALYSIS

The interfacial cracking behavior depicted in Fig. 1 can be efficiently modeled using 3-D enriched crack-tip finite elements [6, 10]. These elements permit direct solution for the interface stress intensity factors K_I, K_{II}, and K_{III}, since the stress intensity factors are included as additional degrees of freedom in the element formulation. Figure 2 schematically depicts two types of initial interface corner cracks between silicon and epoxy used in this study. Figure 3 shows example finite element meshes that were used in this study to compute the initial values of K_I, K_{II}, and K_{III}, for corner cracks at the beginning of a fatigue simulation.

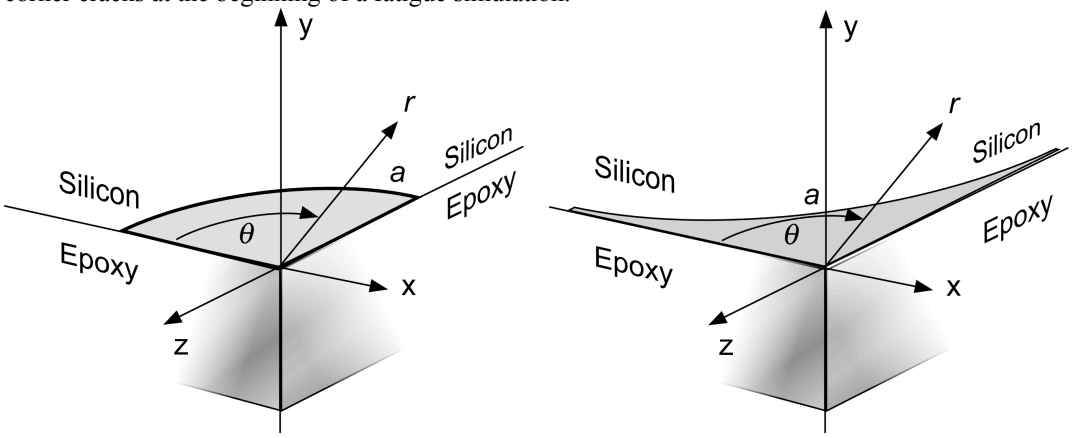

Figure 2: Local coordinates (r, θ) for quarter-circular interface corner crack and cusp-shaped interface corner crack between silicon and epoxy.

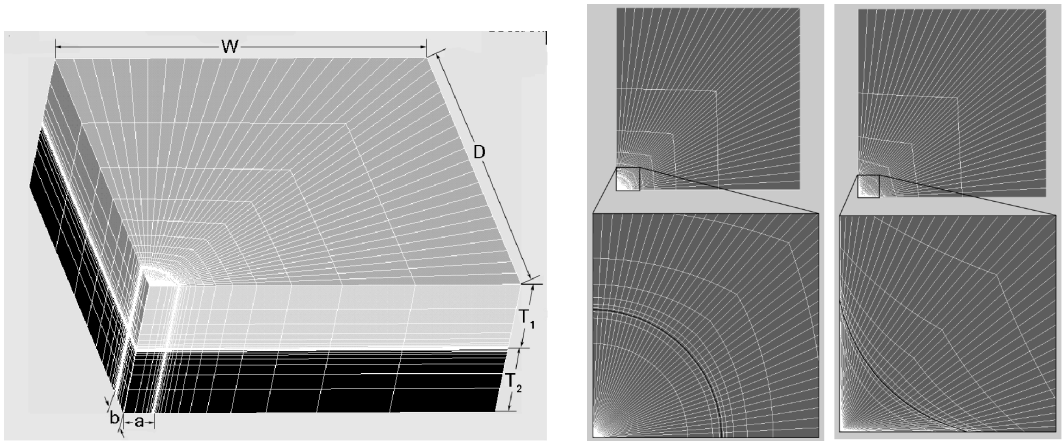

Figure 3: 3-D Finite element model used in simulations and initial mesh for corner crack front (quarter-circular and cusp-shaped crack).

Figure 4 shows the results from a specific finite element calculation for the cusp-shaped corner crack subjected to thermal loading (ΔT=−10°C). Included in Fig. 4 is the total strain energy release rate computed directly from the stress intensity factors using the relationship

$$G = \frac{1}{E_0 \cosh^2(\pi\varepsilon)}\left(K_I^2 + K_{II}^2\right) + \frac{(\mu_1 + \mu_2)}{4\mu_1\mu_2} K_{III}^2 \ , \tag{4}$$

$$\frac{1}{E_0} = \frac{1}{2}\left(\frac{1-\nu_1^2}{E_1} + \frac{1-\nu_2^2}{E_2}\right) \ . \tag{5}$$

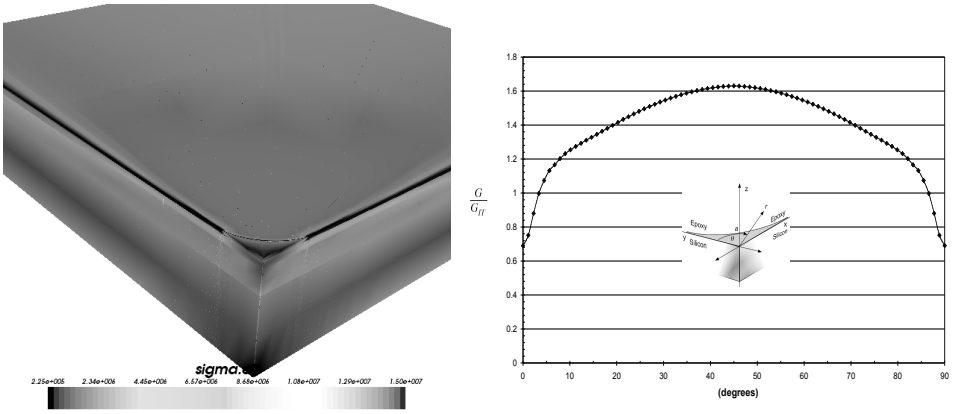

Figure 4: Finite element results for the cusp-shaped corner crack on a BCB/silicon interface subjected to ΔT=−10°C. a) Contour plot of effective stress and b) Normalized strain energy release rate G along the crack front.

3 SIMULATION OF FATIGUE CRACK GROWTH

Simulation of fatigue crack growth starting from the initial geometries depicted in Figs. 2 and 3 consists of the following steps: 1) mesh the cracked geometry, 2) define the crack front elements, 3) compute the stress intensity factors, 4) incrementally advance the crack front nodes using a crack growth rate "law" based on the local stress intensity factors, 5) repeat steps 1 – 4 until the crack reaches a specified size or number of loading cycles.

In general, it's expected that mixed mode fatigue crack growth will depend on both the local changes in the magnitude of the strain energy release rate and the stress intensity factor ratios, e.g.,

$$\frac{da}{dN} = f\left(\Delta G, \psi, \phi\right) \ , \tag{6}$$

where a is local crack length, N the number of cycles, G is given by (4) and

$$\psi = \arctan\left(\frac{K_{II}}{K_I}\right) \ , \quad \varphi = \arctan\left(\frac{K_{III}}{K_I}\right) \ . \tag{7}$$

Unfortunately, data for interfacial mixed mode crack growth does not seem to be currently available as a function of the "phase angles" $\psi$and ϕ given by (7). In the absence of such data and for the purposes of this study, mixed mode crack growth is assumed to be a simple function of the amplitude of the strain energy release rate G, i.e.,

$$\frac{da}{dN} = C\left(\Delta G\right)^m \ . \tag{8}$$

For example, Snodgrass, et al, [11], have reported fatigue crack growth rates on interfaces between an underfill epoxy material, benzocyclobutene (BCB), and silicon, in the form given by (8). For the

case without adhesion promoters, the constants C and m in (8), reported in [11], for fatigue crack growth on this particular interface, are given as C=4.0x10^{-13} J/m^2, m=6.0.

Starting with an initial crack configuration (Fig. 3), fatigue crack propagation based on (8) is simulated by computing ΔG along the entire crack front and advancing the crack front node with the largest ΔG by an increment $\Delta a_{\max}$. ΔN is then computed (8), i.e.,

$$\Delta N = \frac{\Delta a_{\max}}{C\left(\Delta G_{\max}\right)^m} \quad , \tag{9}$$

and then all other crack front nodes i are advanced by an increment Δa_i based on the local value of ΔG using the expression

$$\Delta a_i = \Delta N\left(C\left(\Delta G_i\right)^m\right) \quad . \tag{10}$$

This results in a new crack front geometry that serves as input for a subsequent finite element calculation and new values for K_I, K_{II}, K_{III}, and G along the crack front. Specific details concerning the numerical implementation of this procedure are given in [12], but in general, smooth crack fronts evolve over large relatively distances for sufficiently small increments in the local crack front nodal positions.

2 RESULTS

The crack front propagation algorithm results in a uniform value for the strain energy release rate along the entire crack front after the crack front has advanced a sufficient distance along the interface. Thus, as expected, the shape of the crack front for this "steady-state" condition is independent of the initial crack geometry, e.g., the starter crack shapes shown in Figs. 2 and 3, both converge to the same final crack shape shown in Fig. 5. The magnitude of G for the quarter-circular shaped crack is highest at the free surface and lower in the interior; therefore, the crack front "grows" most rapidly near the free surface for the quarter-circular starter crack. On the other hand, for the cusp-shaped crack, G is higher along the interior part of the crack front than on the free surface, resulting in higher crack growth rates on the central portion of the crack front.

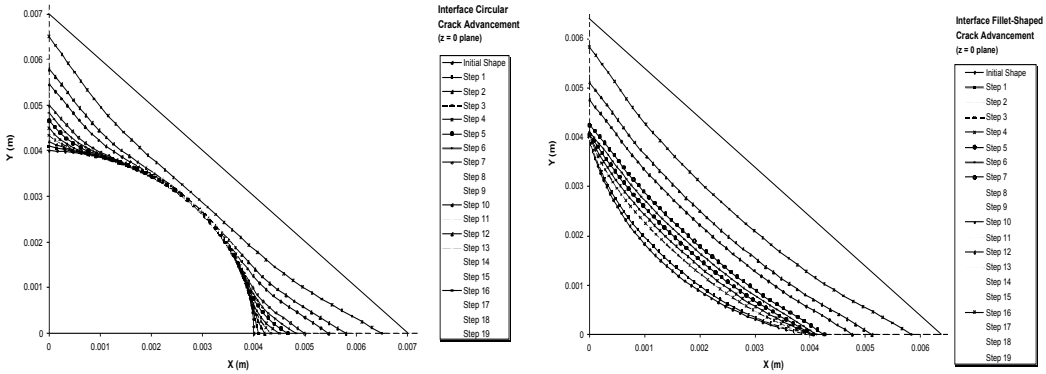

Figure 5: Plot of the nodal points of the advancing quarter-circular and cusp-shaped corner crack. The straight line is to illustrate the curvature of the crack.

ACKLOWLEDGEMENT

The support of the Semiconductor Research Corporation under Contract SRC 826.002 and a grant from General Electric's Corporate Research and Development Center is gratefully acknowledged.

REFERENCES

[1] Wang, J., Zou, D., Lu, M., Ren, W. and Liu, S., "Evaluation of Interfacial Fracture Toughness of a Flip-chip Package and a Bimaterial System by a Combined Experimental and Numerical Method," *Engineering Fracture Mechanics*, **64**, 781 – 797 (1999).

[2] Nied, H. F., "Mechanics of Interface Fracture With Applications in Electronic Packaging," IEEE *Transactions on Device and Materials Reliability*, Vol. 3, No. 4, pp. 129 – 143, (2003).

[3] Xu, A. Q., and Nied, H. F., "Finite Element Analysis of Stress Singularities in Attached Flip Chip Packages," *ASME Journal of Electronic Packaging*, Vol. 122, pp. 301 - 305, (2000).

[4] Begley, M.R., and Ambrico, J.M., 'Delamination of Thin Films From Two-Dimensional Interface Flaws at Corners and Edges', *International Journal of Fracture*, **112**, 205–222 (2001).

[5] Ayhan, A. O., and Nied, H. F., "Finite Element Analysis of Interface Cracking in Semiconductor Packages," *IEEE Transactions on Components and Packaging Technology*, Vol. 22, No. 4, pp. 503 – 511, (1999).

[6] Ayhan, A. O., and Nied, H. F., "Analysis of Three-Dimensional Interface Cracking in Electronic Packages," Advances in Fracture Research, *Proceedings of ICF10*, Editors: K. Ravi-Chandar, B. L. Karihaloo, T. Kishi, R. O. Ritchie, A. T. Yokobori Jr., T. Yokobori, ICF100832OR, Elsevier Science CD-ROM, ISBN 0080440428, December (2001).

[7] Williams, M. L., "The Stresses Around a Fault or Crack in Dissimilar Media," *Bull. Seismological Soc. Amer.*, Vol. 30, pp. 232-237, (1959).

[8] Hutchinson, J. W., and Suo, Z., "Mixed Mode Cracking in Layered Materials," *Advances in Applied Mechanics*, Vol. 29, Hutchinson, J. W., and Wu (eds), T. Y., 63–191, Academic Press, NY (1992).

[9] Herrmann, K. P., Hauck, T., Muller, W. H., Kemmer, G., and Albrecht, H.-J., "Stress Analysis of Thermally Mismatched Solder Assemblies - The Example of A Ball Grid Array Structure," *Proceedings of Micro Materials, Micro Mat'95*, Berlin, 173-179, (1995).

[10] Ayhan, A. O., and Nied, H. F., "Stress Intensity Factors for Three-Dimensional Surface Cracks using Enriched Finite Elements," *International Journal for Numerical Methods in Engineering*, Vol. 54, Issue 6, pp. 899 – 921, 2002.

[11] J.M. Snodgrass, D. Pantelidis, M.L. Jenkins, J.C. Bravman, R.H. Dauskardt, 'Subcritical Debonding of Polymer/Silica Interfaces Under Monotonic and Cyclic Loading', *Acta Materialia*, **50**, 2395 – 2411 (2002).

[12] Herr, A. F., "Automated Simulation of 3-D Crack Propagation on Bimaterial Interfaces in Semiconductor Packages," MS Thesis, Lehigh University, Bethlehem, PA, December 2003.